PROCEEDINGS OF SPIE

SPIEDigitalLibrary.org/conference-proceedings-of-spie

Boosting dispersive spectrograph stability 1000x using an interferometer with crossfaded delays

Erskine, David

David J. Erskine, "Boosting dispersive spectrograph stability 1000x using an interferometer with crossfaded delays," Proc. SPIE 11451, Advances in Optical and Mechanical Technologies for Telescopes and Instrumentation IV, 114512D (13 December 2020); doi: 10.1117/12.2559219

SPIE.

Event: SPIE Astronomical Telescopes + Instrumentation, 2020, Online Only

Boosting dispersive spectrograph stability 1000x using an interferometer with crossfaded delays

David J. Erskine[a]

[a]Lawrence Livermore Nat. Lab., Livermore, CA 94550, USA

ABSTRACT

We demonstrate a key step along a technical route to achieving cm/s scale accuracy for astronomical spectrographs over long (multi-year) time scales, which is critical for the Doppler characterization of earth sized exoplanets, and measurement of small cosmic redshift drift over many years. This same technique is also enabling for searching exoplanet atmospheres for biosignificant molecules in direct planet imaging using otherwise insufficiently low resolution and drift prone dispersive (grating or prism) spectrographs. Using a new method called "crossfading" for externally dispersed interferometers (EDI) to get highly robust spectra, we recently demonstrated a factor of 1000x reduction in the net shift of an EDI measured ThAr line to a deliberate simulated wavelength translation of the detector. This 1000x gain in disperser stability can be combined with conventional stability gains afforded by fiber scramblers, vacuum tanks, and thermal control, to provide an additional 1 to 3 orders of magnitude reduction in the net PSF shift drift. Crossfading combines high and low delay fringing signals that react oppositely in phase to cancel their net reaction to a detector wavelength drift. This can be implemented by an interferometer addition to a facility spectrograph.

Keywords: High resolution spectroscopy, Doppler radial velocimetry, Expolanet detection, Cosmic redshift drift, Laser frequency comb calibrator, Externally Dispersed Interferometry, Dispersed fixed delay interferometry, Spectrograph stabilization

1. SYNOPSIS: CROSSFADING-EDI ROBUST TO SPECTROGRAPH DRIFT

Synopsis: a significant instrumental error for dispersive (grating or prism) spectrographs is uncontrolled drift Δx of its focal point (point spread function, PSF) relative to its detector pixels. This can prevent achieving photon or detector limited performance[8] for high resolution spectroscopy and Doppler velocimetry in a variety of science and engineering fields. A hybrid technique of externally dispersed interferometry (EDI)[1–4,7,9–16] has been used as an inexpensive and compact alternative for Doppler and high resolution spectroscopy, and has been used by other researchers to find exoplanets[17–19] around stars HD102195 and HD87646 in 2005 and 2016. The EDI can be formed from most spectrographs, after their construction, by insertion of a small interferometer in series with its input beam.

The EDI was already known for its excellent stability properties. We have recently discovered improvements in the apparatus design and data processing, called "crossfading" that dramatically improve its stability to a drift Δx by to one to three orders of magnitude. Figure 1 shows a demonstration producing a 1000x reduction of reacting shift to a Δx on a measured ThAr spectral lamp line whose data is artificially drifted– the EDI output (red peak) is virtually stationary. The crossfading technique uses pairs of interferometer delays, rather than a single delay (as used by the basic EDI), as well as strategically chosen weights during data processing that cancel error signals among each delay pair. We envisage improving the resolution and stability performance of facility spectrographs by introducing small interferometers prior to their entrance slit. The increased data processing complexity, and the increased flux losses due to added optical surfaces are penalties, but outweighed by the dramatic improvement in signal to noise ratio due to decrease in the instrumental noise.

The crossfading EDI advantages can be combined with conventional mitigations (fiber scramblers, thermal control, vacuum tanks etc.) to multiplicatively boost the net spectrograph stability several orders of magnitude beyond what can be achieved by conventional mitigations used alone.

Author information:
D.E.: erskine1@llnl.gov

Advances in Optical and Mechanical Technologies for Telescopes and Instrumentation IV,
edited by Ramón Navarro, Roland Geyl, Proc. of SPIE Vol. 11451, 114512D
 · doi: 10.1117/12.2559219

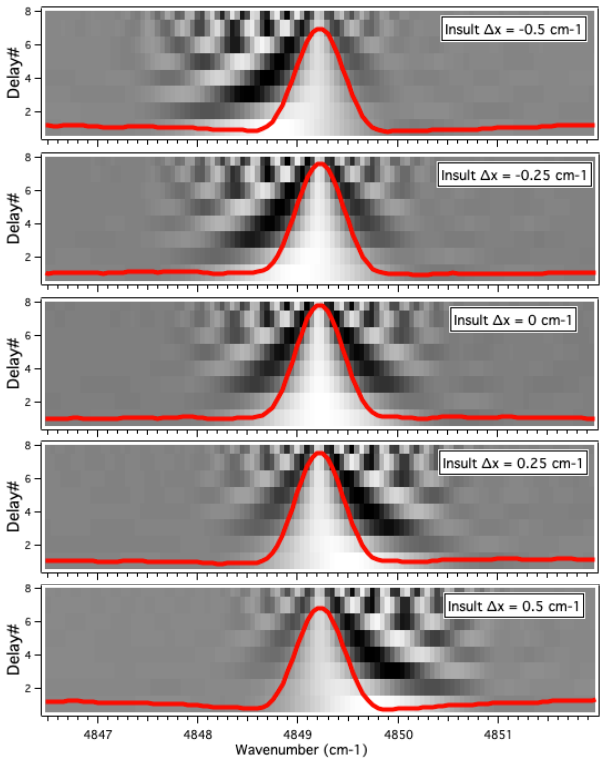

Figure 1. Synopsis: using an externally dispersed interferometer (EDI) with at least two overlapping delays, one can strategically choose weights of a wavelet sum during analysis to almost perfectly cancel the effect of unwanted drift (insult Δx) of the dispersing spectrograph. In this simulation using artificially imposed Δx on measured EDI data of a ThAr lamp at the Mt. Palomar Hale telescope, a reduction by ∼1000x in final ThAr peak position change is achieved for an insulting shift of -0.5 to 0.5 cm^{-1}. The technique, called "crossfading EDI", can be combined with conventional mitigations (fiber scramblers, thermal control, vacuum tanks etc.) to multiplicatively boost the net spectrograph stability several orders of magnitude.

2. MOTIVATION: SPECTROGRAPH DRIFTS

Modern astrophysics demands extremely stable wavelength measurements, such as few cm/s scale Doppler radial velocimetry for earth-like planet detection,[8] and for multi-year cosmic redshift drift measurements.[21,22] Stable measurements are also needed for remote sensing for identifying molecular species spectroscopically on an airborne or space-borne platform enduring the vibrations and accelerations of flight, while still being compact and lightweight. Raman spectrometers identifying molecules for biomedicine can suffer from drift when engineered for compactness and portability rather than stability.

Dispersive spectrographs (grating or prism) are often used to make these measurements. The chief instrumental challenge is often not spectral resolution in resolving a feature, or large photon noise due to insufficient flux, but often lack of wavelength stability. Reference 8 describes some astrophysical high resolution spectrographs whose low noise performance has a floor limited by instrumental errors rather than photon noise (eg. their Fig. 5). The point spread function (PSF) of conventional spectrographs can drift in position (Δx) and shape under thermal changes to the diffraction grating, fluctuations of air internal and external to spectrograph, a changing pupil or gravity vector as target moves across the sky, and flexure of optical fibers (creating mode changes in profile) if fibers are used to communicate the light.

Conventional means for mitigating PSF drift such as thermal control or vacuum tanks reduce the "insult", Δx, which is the drift appearing at the detector. The error in the output spectrum is $\delta\lambda_{out}$, or in our preferred dispersion variable for interferometry, wavenumbers $\delta\nu_{out}$, where ($\nu = 1/\lambda$ in cm^{-1}, and $\delta\nu = -\delta\lambda/\lambda^2$). (The ν is preferred over λ since the interferometer transmission $T = (1/2)(1 + \cos 2\pi\tau\nu)$ is periodic in that variable,

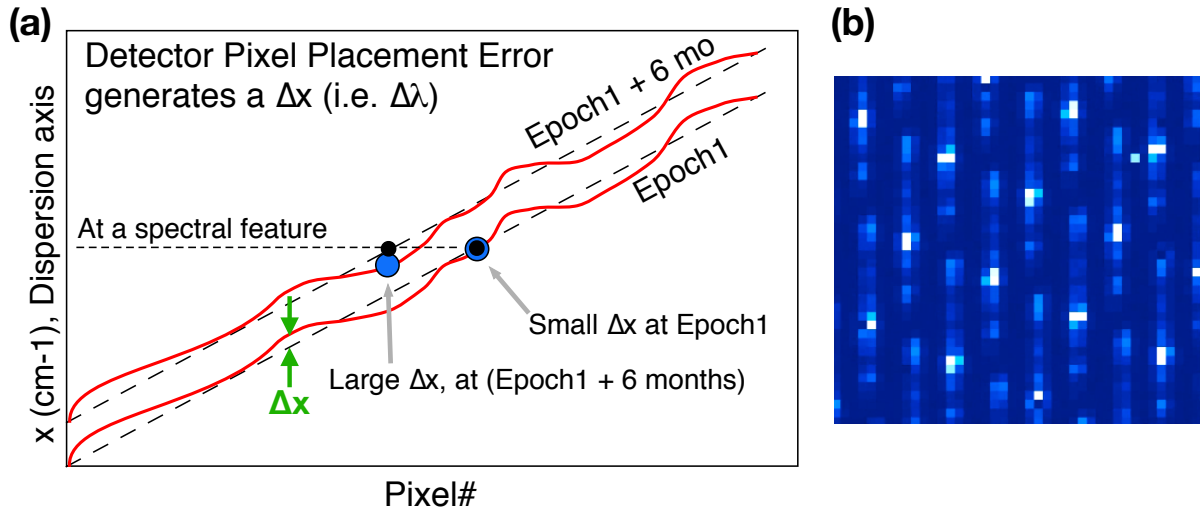

Figure 2. (a) A pernicious type of error is misplacement of detector pixels during manufacture, since it affects spectrographs that are otherwise optically ideal. The insult Δx can vary irregularly and in bipolar manner with wavenumber, and is not removed by conventional mitigations such as fiber scrambling etc. The Δx can vary with date from a large barycentric Doppler component as the Earth revolves around the sun over 6 months, or if different rows of a detector are used, or if a detector fails and is replaced. Fortunately, this error type is easily be corrected by crossfading since the same "baked in" Δx pattern is automatically applied to each delay of a sequential multiple-delay interferometer such as T-EDI.[1–4] (b) An example challenging drift problem at the Gemini Planet Imager integral field spectrograph[5] (small snippet of data shown). This has many close packed spectra, one for each spatial portion of a target. Due to the low resolution and sparse density of pixels, the ∼1 pixel drift due to changing gravity vector[6] would generate a significant wavelength shift. This is a barrier to using GPI to characterize exoplanets at high resolution spectroscopically, but with which EDI can help regarding both spectroscopy[7] and stability.

where τ is the interferometer delay or path length difference in cm. The τ has a slight dependence on ν due to changing refractive index of the glass etalons used to form the delay, and this is calibrated into our software.) For purely dispersive spectrographs, $\delta\nu_{out} = \Delta x$, since the output spectrum is directly linked to position of features on the detector.

Conventional means for mitigating PSF drift include vacuum tanks, thermal insulation and control, adaptive optics, fiber optic scramblers. Often the former are bulky or heavy, precluding airborne or space-borne platforms. The use of spectral calibrants (iodine cells, ThAr lamps) simultaneous with the input stellar spectrum is very important, but by itself may not completely remove an error, because the spectrograph optical behavior and/or detector pixel position may not be perfectly uniform along the dispersion axis.

A laser frequency comb calibrant is useful but typically expensive. Importantly, because the laser calibrant adds to the input spectrum rather than multiplies it (such as an iodine vapor absorption cell), it is difficult to ensure that the calibrant illuminates exactly the same pixels detecting the stellar spectrum. Mismatch in illuminating different pixels detecting calibrant and stellar spectra can lead to errors (10^{-5} pixel precision corresponds to the 3 cm/s needed to measure the 10 cm/s motion of an earth-like exoplanet, given a typical 3 pixels per 10 km/s stellar linewidth scaling of spectrographs). Secondly, there are analysis difficulties when an additive calibrant is steady in amplitude while the input spectrum fluctuates, especially since the fluctuation could be ν dependent.

A particularly pernicious error type is irregular placement of detector pixels (pixel registration error) from manufacturing variability (Fig. 2). This forms an insult Δx which varies with wavenumber and is irregular and bipolar. These misplacements can be milli-pixel in magnitude (corresponding to 300 cm/s) and thus be limiting for Doppler velocimetry of small planets. It is extremely challenging technically for dispersive spectrographs to achieve 10^{-5} pixel stability over years time scale.

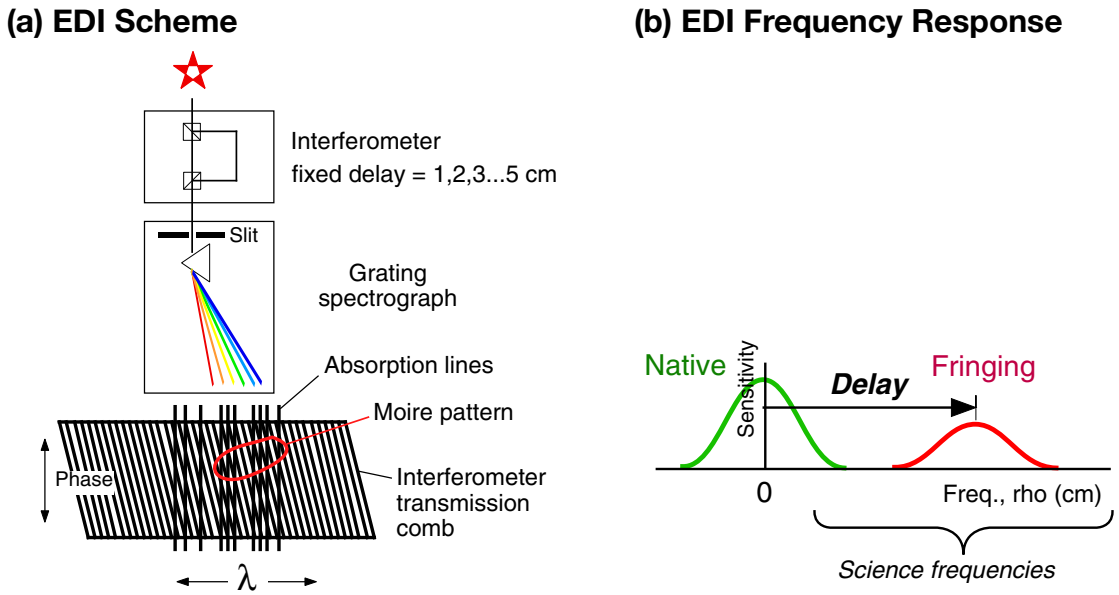

Figure 3. (a) Externally dispersed interferometer scheme: a fixed delay interferometer is crossed with a disperser. The sinusoidal transmission of the interferometer creates moiré patterns whose phase encodes Doppler velocity and shape encodes the spectrum's shape (after shifting up in frequency). (b) Heterodyning (multiplication of a signal by a sinusoid) shifts the native spectrograph sensitivity peak (green peak at zero) up to a higher frequency peak (red) where science frequencies typically reside, by an amount equal to the interferometer delay τ, and halved in amplitude. Frequency in units of features per wavenumber (cm^{-1}), conveniently has units of delay, units of cm.

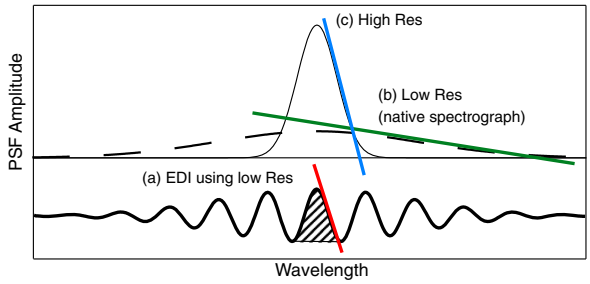

Figure 4. (a) The EDI has an instrument response in dispersion space (wavenumber or wavelength) in the shape of a wavelet (i.e. Fourier transform of frequency response Fig. 3[b]). The interior shape is very stable, being a sinusoid having only three degrees of freedom (phase, period, amplitude), which makes it ideally suited to making precision wavelength measurements. In contrast, a conventional spectrograph instrument response (b)(c) has 100s or more degrees of freedom, at least one per grating groove, which makes it more difficult to make an accurate wavelength measurement. For the EDI, the steep slope of the instrument response desired for high Doppler sensitivity is supplied by the slope of an interior sinusoidal fringe (red line in [a]), controlled by the interferometer delay, and this slope can be similar to a high resolution conventional spectrograph (blue line in [c]). The envelope of the EDI wavelet shape is the same as the conventional spectrograph (dashed curve [b]) with which it is used in series, which is often low resolution.

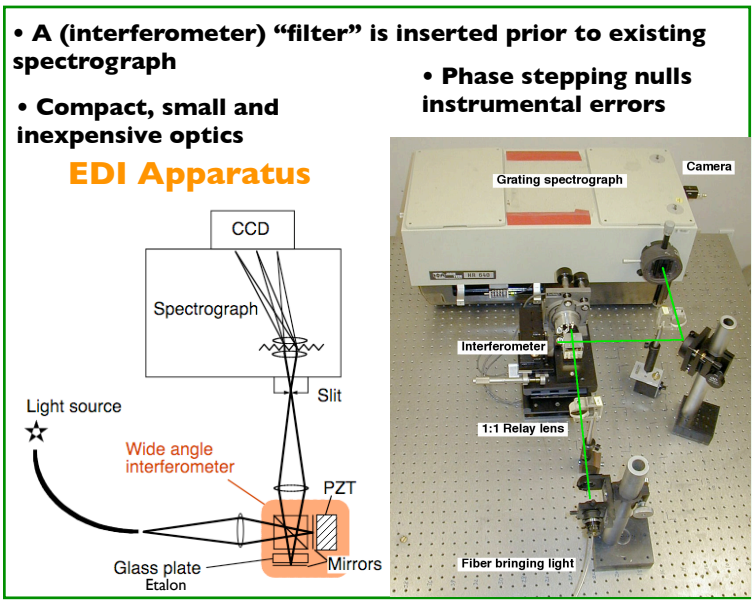

Figure 5. Schematic (left) and photo (right) of an early single-delay EDI built by a 1998 project at Lawrence Livermore Nat. Lab. from off-the-shelf components and tested on sunlight,[11] a stationary backlit bromine absorption cell,[10] and starlight.[20] Even though it had no environmental controls (open air optical paths) it achieved stability, measured by comparing backlit bromine against iodine absorption spectra, of 0.76 m/s over 20 min, 1.2 m/s over 3 hrs, 2 m/s over 11 days,[10,20] and measured the 12 m/s amplitude tugging of the moon on the Earth with 8 m/s scatter over 1 month using sunlight[11] (Fig. 7). The dispersive grating spectrograph was a Jobin-Yvon HR640 (0.7 m length) with maximum Res ∼20,000 into a 13 nm band near 513 nm. The entrance slit was often widened to accept more light but at lower resolution. The moiré phase can still be reliably measured at lower disperser resolutions. Figure from Ref. 13.

This irregular spatial pixel misplacement is not mitigated by fiber scrambling, thermal control, or vacuum tanks (although these can mitigate other types of insults). This can potentially also vary with time if during a different epoch the entire detector is accidentally displaced, or if the entire spectrum is shifted by a different barycentric Doppler component, such as for observations 6 months apart. Cosmic redshift drift measurements, and Doppler measurements of earth-like planets at earth-like orbit sizes also require making cm/s scale measurements over several year timescales. Over these long timescales it is possible detectors can fail and need to be replaced, and the replacement detector will have different pixel misplacements having a different error Δx.

An example potential application of a crossfading-EDI is the spectrograph for the Gemini Planet Imager (GPI), which analyzes light from direct imaging of exoplanets and other objects. The spectrum is dispersed over very few (∼20) pixels at very low (∼50-100) resolution.[5] Drifts in wavelength calibration[6] due to the changing direction of the gravity vector (as the telescope follows the object in the sky over long exposures) can be ∼1 pixel. This is a barrier to using GPI to characterize exoplanets at high resolution spectroscopically, but with which EDI can help regarding both the spectral resolution[7] and stability.

3. SOLUTION: EXTERNALLY DISPERSED INTERFEROMETRY

While we recommend using conventional mitigations when affordable, we propose that dispersive spectrograph stability can be further improved by 1 to 3 orders of magnitude by inclusion of a Michelson interferometer in series, as in EDI. This technique has been used for precision Doppler radial velocimetry and high resolution spectroscopy,[1–4,7,9–16] and other researchers using the technique[19] (that they call "DFDI") have discovered exoplanets[17,18] around stars HD102195 and HD87646 in 2005 and 2016. The technique is mathematically related to, but differing in its practicalities, to dispersed Fourier Transform Spectroscopy.[23] Externally dispersed interferometry differs in behavior from internally dispersed interferometer techniques such as spatial heterodyne spectroscopy (SHS),[24] having gratings internal to the interferometer, which can have extremely high resolution

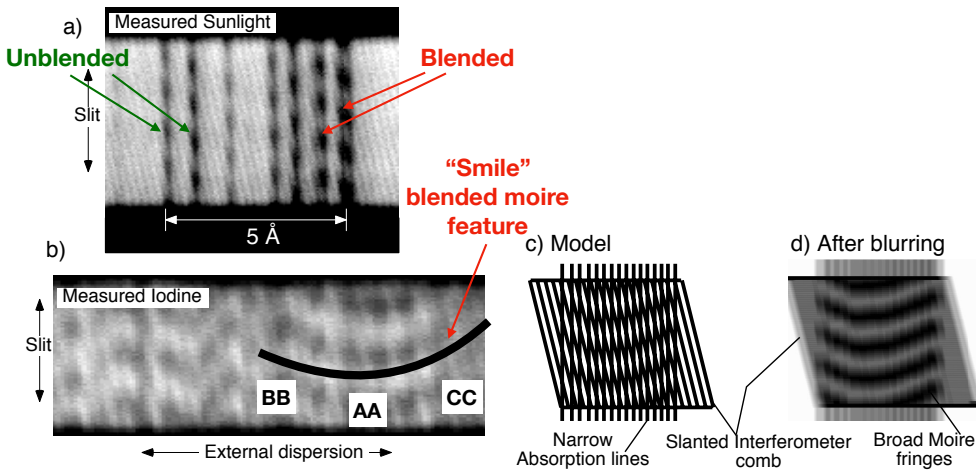

Figure 6. Fringing spectra measured by the 1998 EDI apparatus (Fig. 5) on sunlight (a), and iodine (b) reference spectra, showing moiré patterns. Solar snippet is near 508 nm, iodine snippet near 540 nm, and wavelength increases to the left. Interferometer phase is along vertical axis. Unblurred (c) and blurred (d) model of iodine line group. During velocimetry observations solar and iodine would be measured simultaneously on the same pixels. Note the smile-like blended feature (BB to CC) in the iodine moiré pattern due to many nearly periodic closely spaced lines, similar in frequency to the 1.1 cm delay interferometer comb (at AA) but slowly changing. Isolated solar lines (left side of [a]) are very robust to spectrograph drift Δx because the interferometer comb and solar spectra move together. However, blended solar lines (right side of [a]) have an apparent moiré slope and thus would create a phase error for a Δx. Similarly for inclined portions of the blended iodine smile-feature in (b). Being bipolar, most of the phase error cancels out when integrated over the band for a Doppler measurement, but there will be a small remainder which is undesirable. Secondly, the phase error is not uniform, and thus may couple to any non-uniformity in the spectrograph. In spite of this, the 1998 single-delay EDI performed remarkably well (Fig. 7). The crossfading method we propose can cancel this type of error, by measuring Doppler velocities with two slightly different delays, foretelling even better performance. Graphics based on Fig. 5 of Ref. 11.

over a more limited bandwidth. In contrast, EDI's bandwidth is not limited by the interferometer and extends over the native spectrograph's bandwidth.

3.1 Translational Reaction Coefficient

In the EDI method the detailed wavelength determination is decoupled from the spatial scale in the disperser and its drift Δx. Instead, it is determined by the phase of a fringe (intensity measurement) in an interferometer cavity, which is calibrated by a spectral reference such as an iodine cell, ThAr lamp or aforementioned laser frequency comb. The cavity PSF is sinusoidal and has only three degrees of freedom (amplitude, period, phase). This is much easier to control or calibrate than the hundreds of degrees of freedom for a disperser PSF (at least one per grating groove).

Hence the output PSF drift is given by

$$\delta\nu_{out} = \Delta x * TRC = \Delta x / G_{edi}, \tag{1}$$

where TRC is the translation reaction coefficient of the spectroscopic method used, and EDI stability gain $G_{edi} \equiv 1/TRC$. The TRC is the output shift per input shift. For dispersive spectroscopy TRC = 1 by definition.

TRC$\ll$1 for EDI because it does not use the feature's position along the spectrograph detector dispersion axis to determined its detailed wavenumber. Instead it uses the interferometer– specifically it uses the phase of the moiré pattern. The EDI spectrum output is decoupled from the dispersive spectrograph.

Significantly, for EDI using multiple delays we show in a method called "crossfading" (Sect. 10 of Ref. 3) how to theoretically make TRC = 0 for small insults. (Small relative to the spectrograph resolution element, so that fringe phase shifts are small angles and thus the phasor $e^{i2\pi(\Delta x)(\rho-\tau)}$ that rotates the complex value of the Fourier transform in the EDI output, at a frequency $\rho \approx \tau$ set near a delay, is approximately linear in Δx).

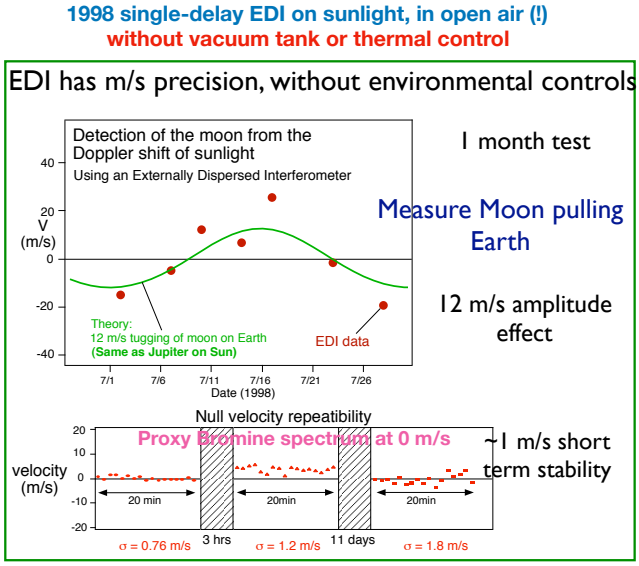

Figure 7. The single-delay 1998 EDI (using open air optics without thermal control for expediency) measured of the 12 m/s amplitude tugging of the moon on the Earth with 8 m/s scatter over 1 month using sunlight.[11] The zero point drift or Doppler velocity repeatability was measured using a bromine absorption cell backlit by white light as a stationary proxy for starlight or sunlight. This light then passes through the usual iodine absorption cell. Repeatability was within a few m/s, even up to 11 days.[10,20] We propose using a pair of overlapping delays and crossfading to improve the Doppler performance over this single-delay result, which is already remarkable considering no environmental controls were used. Adding conventional environmental controls would further improve the performance.

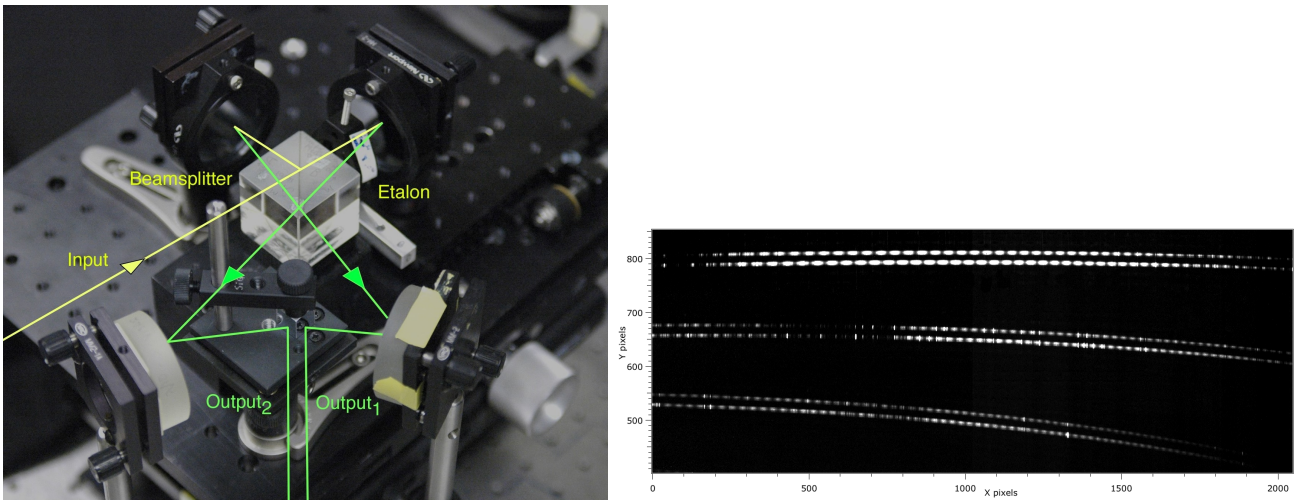

Figure 8. (Left) An interferometer splits light into two complementary phase outputs, both of which can be directed to the spectrograph (but should fall on different pixels). This was done with the first version[15] of T-EDI at Mt. Palomar (2007-9)– note complementary phased combs in echelle data of star GJ 338A (right) using a 0.3 cm delay. The interferometer is ideally lossless, but practical optics has parasitic reflections which can be reduced by high quality anti-reflection coatings. Because the optical delays needed are typically 1-5 cm round trip, produced by 0.5 to 2.5 cm single trip distances, the interferometer can be a few cm in size. Monolithic designs made from glued prisms would be especially compact (see Fig. 7 of Ref. 14).

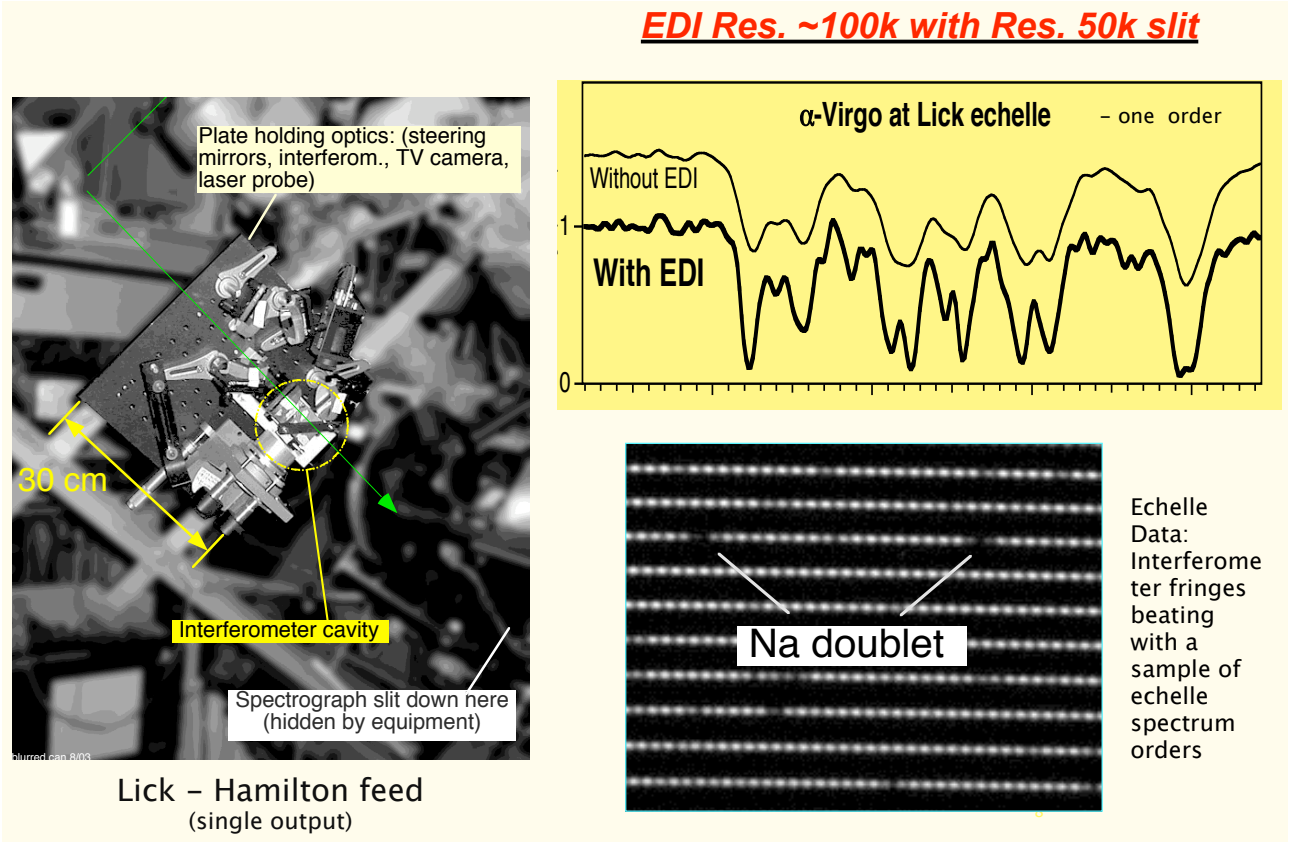

Figure 9. In 2002 we tested a single-delay EDI on the Lick Observatory Hamilton echelle spectrograph, famous for exoplanet observations. We demonstrated (a) we can use a single pixel wide beam and do phase stepping versus time rather than spatially across a slit. (b) Secondly we can boost[12] the spectral resolution of a facility spectrograph 2x with a single delay, without narrowing the slit or changing its grating. (Subsequent demonstrations[1–4] with a multiple-delay T-EDI at the Mt. Palomar Hale telescope 2008-11 demonstrated we can boost the native TripleSpec[26] resolution 10x using 7 delays, from native 2700 to final 27,000.) (Left) The 1.1 cm delay interferometer mounted on a 30 cm square plate temporarily intercepts and then returns the beam from the telescope to the spectrograph entrance slit, without disturbing either system. An even number of reflections makes alignment easy– insensitive to plate orientation. (Top right) Ordinary spectra (thin) and 2x boosted EDI spectra (bold) on star α-Virgo (native resolution 53k boosted to 96k). (Bottom right) Section of 2d echelle multi-order spectrum around the Na doublet. Note periodic interferometer comb embedded in the spectra, which functions as a very uniform calibration spectrum, as well as having the heterodyning property to boost resolution.

In our previous work we showed that the benefit of multiple delays, but without special weights, can achieve TRC ∼1/20 (Fig. 42 of Ref. 3) on a single ThAr line using the same data analysis software used in the project. More recently,[25] and discussed in detail in this report, we further reduce TRC to ∼1/1000 by using strategically chosen weightings to force phase cancellation between each pair of delays for a set of overlapping delays, and made other algorithmic improvements.

The crossfading technique works because under the same detector wavelength drift, EDI signals for a high delay twist in one direction, and for a low delay twist in the opposite direction. For final spectrum frequencies that lie in between a pair of delays (that overlap), we choose weightings that cancel the net phase shift. We do this for every pair of delays for each frequency, up to a limiting frequency of the highest delay.

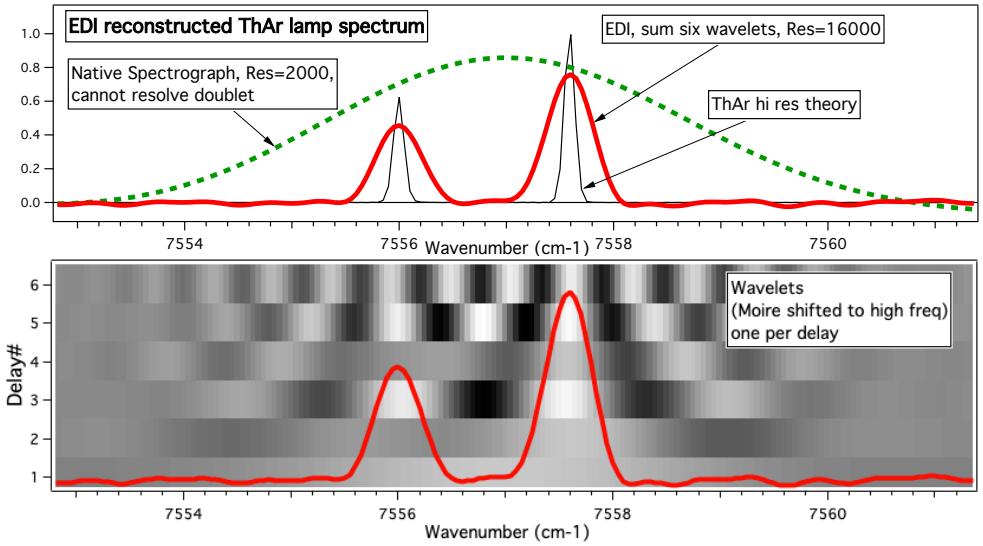

Figure 10. Demonstration of 8x resolution boosting measuring a ThAr lamp at the Hale Telescope (similar to Fig. 5 of Ref. 3). Phase stepped exposures are made at each of six delays, produce moiré and nonfringing (ordinary) spectra. The moiré are shifted to higher frequency in Fourier space by the amount of each delay, to form a set of wavelets (bottom panel). A neighboring ThAr line (off graph at 7532 cm^{-1}) provides phase alignment as the channels are added to form the output (red curves). The nonfringing spectra at Res=2000 (green dash) cannot resolve the doublet (thin black, hi res theory). The EDI reconstructed spectrum (thick red curve) equalized to Res=16000 fully resolves the doublet.

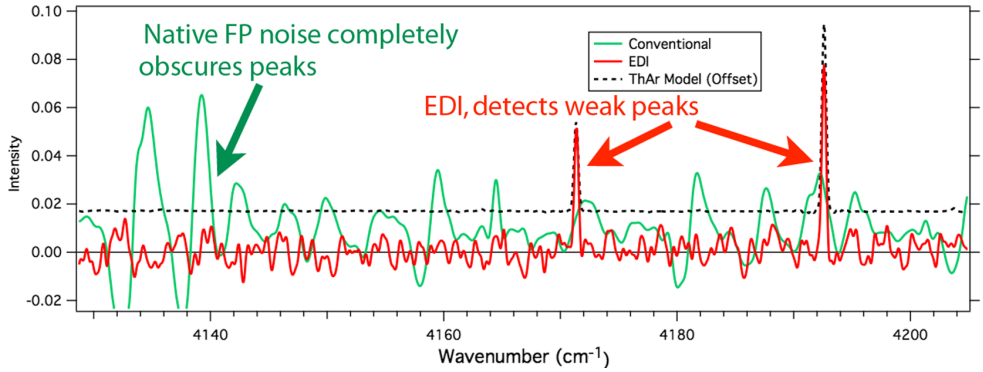

Figure 11. Another practical advantage of EDI is its robustness to fixed pattern noise such as bad pixels, which can plague low light performance. Because it compares at least three exposures, any constant pattern is automatically cancelled. Here T-EDI measures a ThAr lamp (from Fig. 33 of Ref. 3). The TripleSpec native spectrograph (green curve) has so much fixed pattern noise that the two ThAr lines (peaks in black dotted theory curve[27]) are obscured, whereas EDI (red curve) detects them easily.

4. EDI BACKGROUND

Figure 3(a) shows the EDI scheme, where an interferometer with a selectable fixed delay is in series with a dispersive spectrograph. The interferometer has a periodic sinusoidal transmission which multiplies the input stellar spectrum. This embeds a type of calibrant grid on the input spectrum which is automatically detected by the same pixels as the input spectrum.

Fringing spectra exposures contain simultaneously both the fringing component and the ordinary nonfringing spectrum. By taking data in several exposures while the phase is varied (as for echelle spectrographs), or by varying the phase spatially along the spectrograph slit (as for single order spectrographs), the data is taken in a so-called phase stepped manner. During analysis, addition of the exposures cancels the fringes and yields the ordinary spectrum. While subtraction of the exposures cancels the ordinary spectra and reveals the purely fringing spectrum, which are represented by a complex wave. Hence both ordinary and fringing signals are obtained simultaneously from an EDI.

Multiplication of the sinusoidal transmission comb times the input spectrum creates a down shifted heterodyned component, which are seen as moiré patterns. The amount of shift is set by the delay measured in distance units. (Frequency and delay have the same units of features per cm^{-1}, which is cm). High frequency signals, which normally would be too fine for the native spectrograph to resolve, are now detectable through their moiré patterns, which are much lower in frequency and thus resolvable. Figure 3(b) illustrates that effectively, the sensitivity peak of the instrument (green peak centered at zero) has been shifted up (red peak), by amount of the delay τ. The Fourier transform of this red peak at high frequency is the EDI instrument response in wavenumber or dispersion space, which has a wavelet-like appearance (Fig. 4).

Figure 5 shows an early EDI built by the author in a 1998 project, producing stellar, solar, and iodine moiré data (Fig. 6). For expediency we used beams in open air without temperature or pressure control and subject to convection, and the native spectrograph subject to thermal drifts. Because the iodine absorption spectrum is measured simultaneously with the solar or stellar spectra, the detailed value of the interferometer delay can be determined, and one does not need to stabilize the interferometer cavity better than a rudimentary quarter fringe (to prevent fringes from washing out during long exposures). Under minor drifts of the delay, both the iodine and stellar moiré patterns shift phase by the same amount, and one subtracts them to yield a Doppler measurement that is fairly independent of the precise delay value.

Thus it was practical to obtained m/s scale precision of this early EDI in spite of lack of traditional stabilizing mitigations of vacuum tanks and thermal controls. Figure 7 shows that the 12 m/s amplitude component of the moon tugging the earth was measured using sunlight from a rooftop fiberoptic heliostat. Doppler velocity reproducibility was tested using a back-lit bromine absorption cell as a proxy for a stellar spectrum, and was repeatable to a few m/s even up to 11 days. These results are remarkable from an unstabilized instrument, and we expect that inclusion of (a) convention stabilizing mitigations and (b) modern crossfading mitigations would improve the precision even further.

An ideal interferometer does not absorb light but redirects it (depending on its detailed wavenumber) into two complementary phased outputs (as in Fig. 8). Both outputs can be detected by a spectrograph, but necessarily on different pixels (otherwise the fringes cancel). Our early version of the T-EDI interferometer[15] detected both outputs (note complementary phased combs in data of right panel). However, instrumental errors rather than photon limited errors usually dominate our observations, so we often used just one output for convenience.

Figure 9 shows how in 2002 we tested the single-delay EDI on the Lick Observatory Hamilton echelle spectrograph and achieved a resolution boosting of ∼2x on starlight, without altering the spectrograph or using a narrower slit. The interferometer was temporarily inserted into the beam between the telescope and spectrograph entrance slit by mounting on a 30 cm square plate. An even number of reflections on the plate simplified alignment by making it insensitive to slight mis-orientation.

Further resolution boosting beyond 2x can easily be obtained by using multiple-delays, as an 8x-10x boost was demonstrated in the T-EDI project (Fig. 10). Higher boost could have been obtained if we had purchased more glass etalons (which create the delay) to fill the gaps in our delay coverage (and if we had more than 8 positions in the rotary mount to hold them). The boost is determined by the highest delay value.

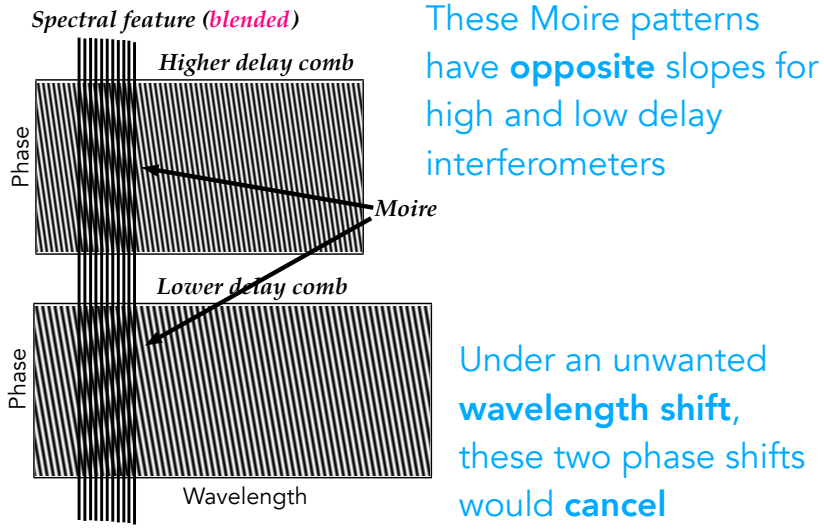

Figure 12. The crossfading idea: have at least two slightly different delays so that the moiré patterns have opposite slopes, cancelling the susceptibility to Δx drift, especially for blended features. This works for the range of frequencies in between each delay of each pair, and when strategically designed weightings are used that account for the instrument lineshape.

Another practical advantage of EDI is that it has extreme robustness to fixed pattern noise (FP) such as bad pixels. Fixed pattern noise often plagues low flux exposures. In the demonstration Fig. 11 the native spectrograph alone (green curve) cannot detect the two ThAr spectral features (black dotted) because of the strong FP noise, but the EDI (red curve) easily detects the features. Because taking data in a phase stepping manner acts like a natural flat fielding process, only features that respond synchronously to the phase dither are detected– any constant background pattern is cancelled.

5. CROSSFADING PAIRS OF DELAY FOR STABILITY

Features can be blended or unblended (isolated).

For isolated features: Measuring isolated narrow spectral lines, such as those on left hand side of the solar fringing spectrum of Fig. 6(a), is very much more robust to drift Δx for an EDI than for a native spectrograph alone. This is because for the EDI the periodic sinusoidal comb is embedded in the input spectrum and drifts along with it. The moiré phase, which determines the perceived wavelength in EDI, only changes when the input spectrum moves *relative* to the sinusoidal comb. Whereas for the native spectrograph the measurement is directly shifted by Δx.

(For an infinitely narrow spectral line which has equal Fourier energy at all frequencies, EDI is perfectly robust. However, for a finite width line which has a Gaussian distribution of Fourier frequencies, there is slightly more energy to the low delay or frequency side of the EDI sensitivity peak than the high side. Thus there can be a slight dependence of moiré phase on Δx, even for an isolated line.)

For blended features: The opposite of an isolated spectral feature is a blended feature, such as on the right side of the solar fringing spectrum in Fig. 6(a), or the smile-like features in the iodine fringing spectrum (Fig. 6[b]). Blended features create slanted moiré, which can create a phase (vertical) error when translated (horizontally) by Δx. These errors are bipolar and thus tend to cancel each other out when summing Doppler velocity over a broad band. However having them is undesirable, because their irregular bipolar placement might couple to irregularities in the spectrograph having similar length scale, potentially creating a net error.

Since the precision demanded of measuring an earth-like exoplanet (10 cm/s amplitude), or measuring a few cm/s cosmic red shift over a few years is so severe, even when using a calibrant such as an iodine cell there could be significant residual instrumental errors, as discussed in Ref. 8. Hence we seek to cancel or dramatically reduce any potential error due to drift Δx, in spite of use of simultaneous calibrants.

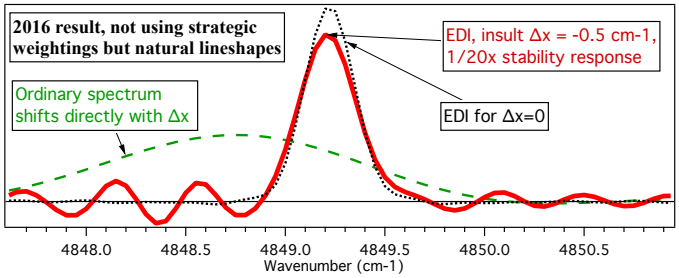

Figure 13. Previous demonstration reported in 2016 (Fig. 42 of Ref. 3) using simple unweighted (natural lineshape) summation on multiple delay ThAr spectral lamp data with an artificial shift of Δx=-0.5 cm^{-1} applied to each delay's data. A 20x stability gain resulted, since the EDI peak (red curve) shifted -0.025 cm^{-1} relative to the Δx= 0 case (black dots). In contrast the conventional spectrum (green dashes) shifts directly with Δx.

This error can be dramatically reduced or eliminated by the new technique of crossfading by the use of pairs of slightly different delays. Figure 12 is a graphical demonstration of how an unwanted spectrograph wavelength shift would create oppositely slanted moiré blended features, and thus opposite phase shifts under the same Δx.

The concept of crossfading was introduced in Ref. 3 in 2016 but not fully explored then. Ideal crossfading would involve choosing weights that would reshape a lineshape to improve cancellation between two overlapping delay signals. However we realized that even without weights, the overlapping that occurs with the natural lineshape of two neighboring delay signals provides some "accidental" crossfading. This produces a reduction, although not to zero, of the reaction to a drift Δx. This was demonstrated in Fig. 13 (originally Fig. 42 of Ref. 3) on a measured ThAr line whose data was artificially shifted by -0.5 cm^{-1} and a reaction of -0.025 cm^{-1} was observed– hence a stability gain of 20x.

Since 2016 we have improved crossfading in this test case to have 50x better cancellation (1000x instead of 20x), by use of strategically chosen weights and some algorithmic improvements. The 2019 demonstration on the same line, but with strategically chosen weights, is shown in Fig. 14. Figure 15 shows the sum wavelet peak position Reaction vs Applied Δx for a range of insults, and for two different weightings schemes L and S, optimized for large (L) and small (S) insults. (For small insults the sinusoidal behavior in the phasor $e^{i2\pi(\Delta x)(\rho-\tau)}$ is linear, and a better stability gain can result but at risk of worse behavior for large insults). This graph confirms the ∼1000x reduction in peak reaction per insult Δx behavior (slope of green dotted line), especially for small Δx. The slight asymmetry of the graph is likely due to our use of experimentally measured data that may not have been perfectly restored to their $\Delta x = 0$ positions prior to the applied Δx.

6. BEHAVIOR IN FOURIER SPACE

6.1 Fourier Behavior of Conventional Spectrograph

Figure 16 is a plot of the Modulation Transfer Function (MTF), that shows the effect of Δx on the Fourier response of both (a) a conventional spectrograph, and (b) an EDI. For the conventional spectrograph (a) a standard mathematical relation says that a shift Δx in the spectrum rotates its complex Fourier value by phasor $e^{i2\pi(\Delta x)\rho}$, where ρ is the frequency variable. For small Δx, the linear growth of the rotation angle of $2\pi(\Delta x)\rho$ radians is depicted by the red inclined line from the origin. This depicts angular reaction or imaginary component (since the magnitude changes slowly, as a cosine to that angle).

The green region represents high frequencies where the science (Doppler shifts, or positional information of narrow features) typically reside. The black dot in the green region of (a) represents the large amount of reaction to a Δx for the conventional spectrograph, to be compared with the near zero amount of the black dot for the EDI in (b).

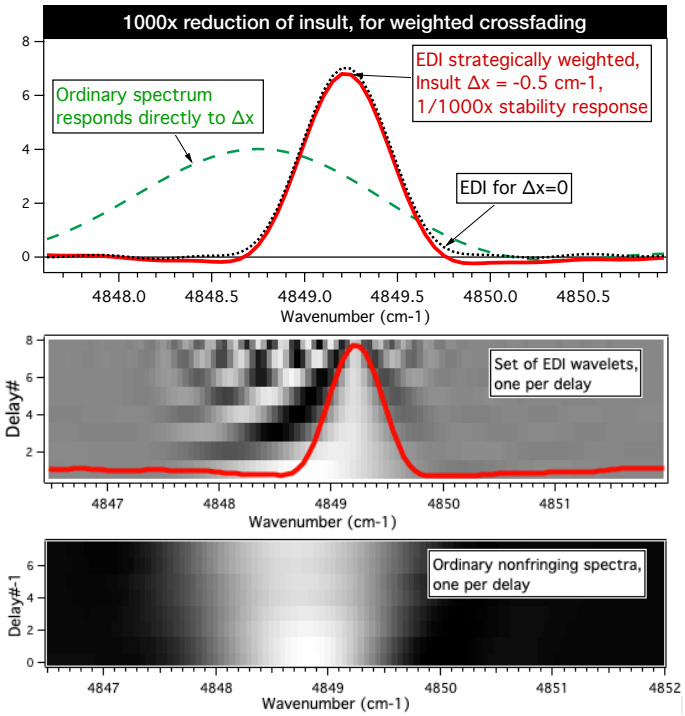

Figure 14. Improved demonstration in 2019[22,25] using our strategically weighted crossfading algorithm on the same ThAr data as Fig. 13 produces 1000x stability for the net EDI peak (red curve) under an artificial insult Δx. This is an improvement of 50x over the previous 20x stability, by use of strategic weights and other algorithmic improvements. The weights were calculated from a neighboring spectral line (4764 cm^{-1}) acting as an ersatz calibrant, then applied to the subject line here at 4849 cm^{-1} to achieve 1000x reduction of the applied translational insult. About 0.001 cm^{-1} peak shift was observed comparing Δx = -0.5 to +0.5 cm^{-1}. (Upper panel) The black dotted curve is the Δx= 0 case. Ordinary spectrum (green dashes) responds directly to Δx. (Middle panel) Net EDI is a sum of multiple wavelets, each from a different interferometer delay (etalon). (Bottom panel) ordinary spectrum from each delay channel. These shift directly with Δx.

6.2 Fourier Behavior of EDI

For EDI in panel (b), the heterodyning shifts the sensitivity peak from the origin to higher frequency by delay τ. A spectral shift by Δx causes the Fourier transform of the EDI output spectrum to rotate by $e^{i2\pi(\Delta x)(\rho-\tau)}$.

Thus the red EDI reaction line goes through zero height at the center frequency of the peak, at $\rho = \tau$. At this frequency the moiré that is detected is perfectly broad– we are downshifting a feature of frequency τ to near zero. And it makes sense that it has near zero reaction to Δx, since broad, constant, features have little slope. Thus the black dot in (b) at the center frequency $\rho = \tau$ has perfect robustness to drift Δx, and TRC=0.

However, general signals occupy a range of frequencies, not a single frequency, so the net TRC for EDI is an average of behavior for a range of frequencies around the center of the peak. Note that the polarity of the reaction line flips across this peak. Hence for a uniform distribution of Fourier energy, such as generated by an infinitely narrow spectral line, the sum of reaction will be nearly zero. Hence for a unblended spectral line, it is nearly perfectly robust to drift.

This explanation in frequency space is a companion to the dispersion space explanation that, since the embedded sinusoidal comb shifts the same amount as the input spectrum, there is no relative shift and hence no moiré phase shift. So for unblended isolated features the EDI has nearly TRC ~0, in comparison to the conventional spectrograph where $TRC = 1$.

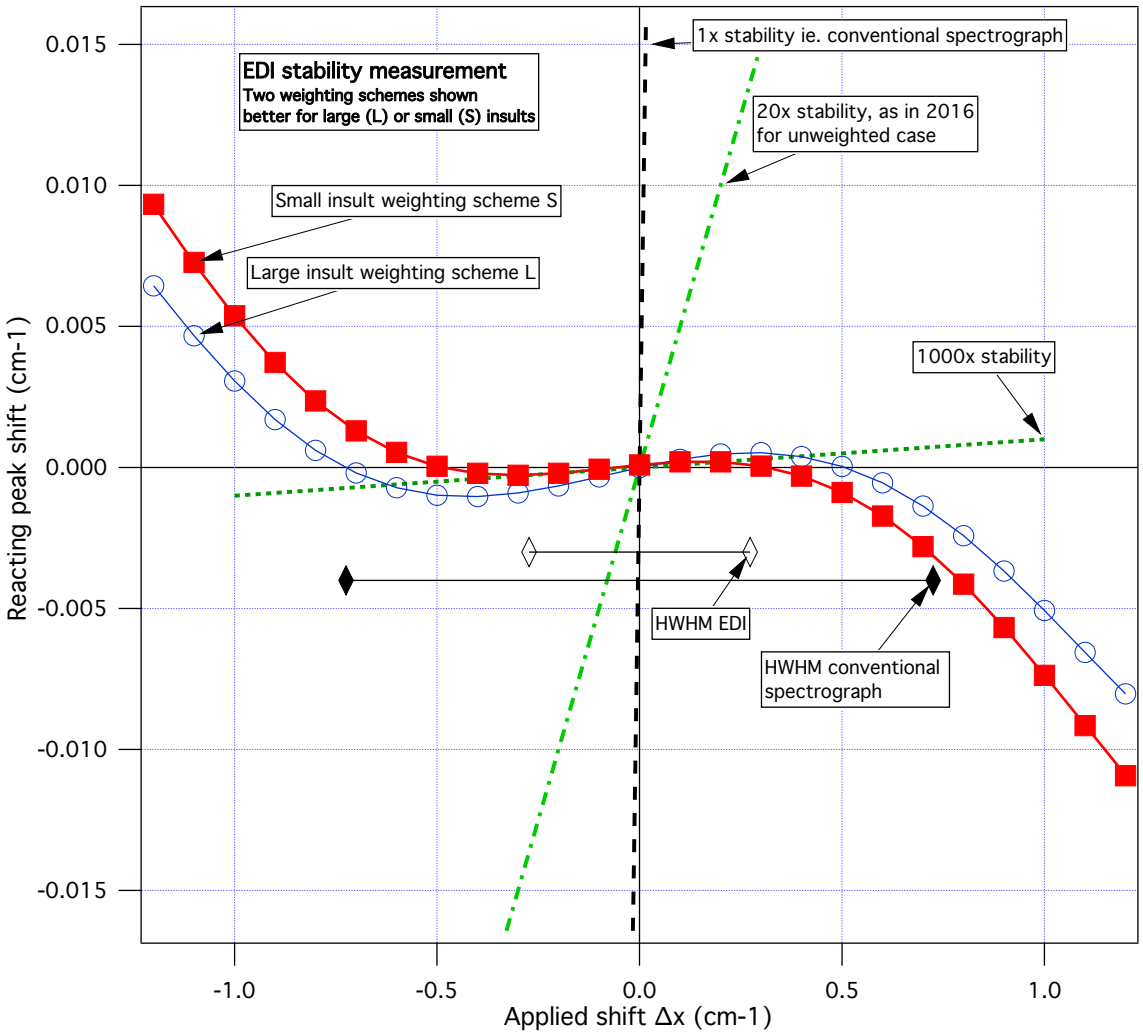

Figure 15. Reaction vs applied drift insult Δx for the crossfading algorithm, using two weighting schemes optimized for small (S, red squares) and large (L, blue open circles) insult ranges of ± 0.2 and ± 0.5 cm^{-1}, respectively. We see that the assumption of a proportionality $\delta\nu_{out} = TRC * \Delta x = \Delta x / G_{edi}$ is valid for small Δx. In reality the sinusoidal behavior of the imaginary component of vector construction is nonlinear with large phase angle arguments, when Δx approaches the half width at half max (HWHM) of the native spectrograph (black diamond) or EDI (open diamond). The weightings were calculated on behavior of a neighboring ersatz calibrant line of 4764 cm^{-1}, and then applied to the subject line of 4849 cm^{-1} to calculate the reaction of EDI output peak. The approximately 1000x reduction in peak reaction per insult Δx is confirmed (green dotted line), especially for small Δx, and is definitely an improvement over the earlier unweighted result of 20x (green dot-dashed line), or conventional 1x (black dashed line). We envision iterating using weighting L to reduce the initial Δx to a smaller value before re-applying with weighting S. Closed and open diamonds indicate HWHM of native and EDI processed PSF, 0.725 cm^{-1} and 0.27 cm^{-1} (R=3300 and 9000).

6.3 Crossfading Cancels Net Reaction

For blended features the frequency distribution is potentially non-uniform about $\rho = \tau$, and thus could generate a small net reaction error. Thus the point of crossfading is to cancel the net reaction so that TRC is as small as possible, even for blended features.

Figure 17 shows that by combining the reactions of multiple delays, rather than single delay, the net reaction could be reduced to zero over a range of frequencies. The reaction line for an individual delay flips polarity at its delay value. Hence two overlapping delay peaks will tend to cancel their net reaction when the high and

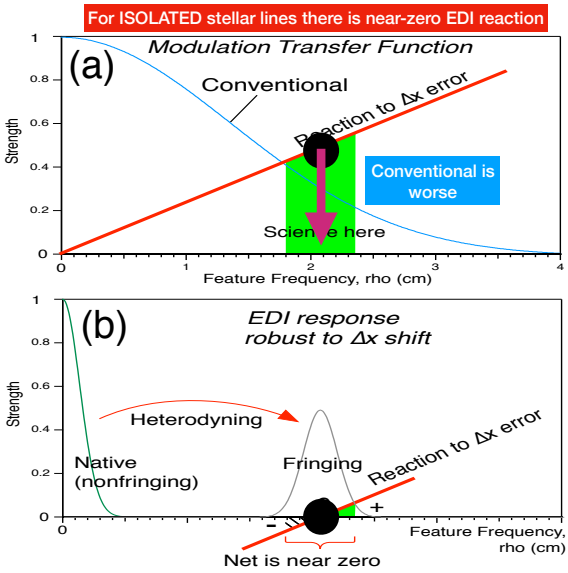

Figure 16. Effect of a wavenumber (or wavelength) drift on the Fourier response, for conventional (a) and EDI (b) techniques, for the case of an isolated narrow feature (unblended). The reaction of the conventional spectrograph (black dot in [a]) is significantly larger than the near-zero reaction of EDI [b]. An isolated very narrow feature produces a smooth distribution of frequencies in the region of the EDI sensitivity peak. These nearly cancel, producing near-zero TRC (translational reaction coefficient), i.e. very high stability gain.

low frequency sides combine in a weighted sum during data processing. By choosing weights we can ensure this cancellation. Figure 18 shows the frequency region in between two delays, and how the complex value of the net frequency response, represented by two vectors, sum to form a small angle vector (b), which can be zero when (c) the weights are adjusted.

7. HOW WE CALCULATED WEIGHTINGS

Reference 3 in Sections 4-7 describe our EDI algorithm for processing of echelle fringe spectra data, performing heterodyning reversal, summing and equalizing the wavelets to form an output spectrum, and Sect. 10 some theory of crossfading.

7.1 What is New to the Algorithm Since 2016

Since the introduction of the crossfading concept in 2016 (Sect. 10 in Ref. 3) we have made algorithmic improvements that have made it more practical:

– Analysis in output space rather than input space, that is, working after, not before the heterodyning reversal has been applied to the moiré data. This way if there is an unknown effect or process that affects the result, it is automatically considered by the weight choice.

– Use of the exact behavior of the Fourier transformed instrument response to a displacement (Fig. 19) and not an idealized small angle approximation for it. This allows it to better handle large insults.

– Use of a minimal number of points for the region of interest around the feature. We use 200 points instead of full order size of 28000 (the raw data is resampled to 0.05 cm^{-1} per point). The smaller number of points reduces the number of independent weights that must be selected by 140x, to only about 17 values (see weight results Fig. 20(b)), since to achieve the 9000 goal resolution (after equalization) we use a delay range from 0 to 1.8 cm and the Fourier transform of the 200 points yields a frequency spacing of 0.1 cm. Processing the whole band then involves scanning this smaller region of interest repetitively across the band.

– The search for the best weight ratio at each frequency ρ is considered independently of other frequencies– the shape of the line is not considered. Thus during the crossfading we only need to pay attention to the relative

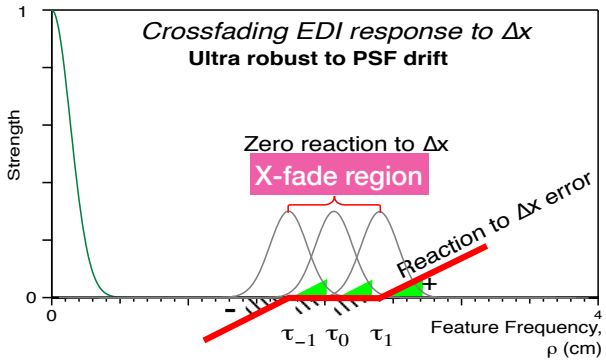

Figure 17. With multiple delays (three shown), rather than single delay EDI, the net reaction to an insult Δx is dramatically reduced to near zero over a *range* (between delay centers) when the positive and negative portions of the peaks overlap and appropriate weightings are used. This is called "crossfading".

sizes of the two weights, not their absolute size. (Once the two delay signals are combined, the signal will be further reshaped during the usual equalization step into a Gaussian having goal Res = 9000 and this removes dips between delays. Because our range of delays is finite, the high frequency edge of any Gaussian will overlap to some degree absent frequencies not covered by delays, producing some ringing. Reducing the goal Res reduces ringing at the expense of spectral resolution– 9000 is a good compromise.)

7.2 Requirement of Pairwise Same Insult

A condition of ideal crossfading is that the same Δx applies to both delays of a pair, so that weightings calculated under that assumption produce cancellation. If the Δx slowly changes, only the portion equal on both sides of the pair will cancel. (Alternatively, if Δx grows in a predictable manner one could calculate weightings that anticipate that.) Only the time needed to complete an individual pair of delays, not the time to complete all delays of a large multiple delay set, is what is compared to the drift time scale.

The detector pixel misplacement error is ideally suited for removal by crossfading by a sequential multiple-delay EDI (like T-EDI[1,3,4]) that uses the same rows on the detector for each delay in a sequence of exposures while changing among different delays, since the same pattern in Δx applies for each delay.

A single-delay EDI where the delay overlaps the native spectrograph sensitivity peak, indicated by partially resolving the comb in the data, (as in several of the early EDI's[10–12,20]) has the interesting property that Δx will automatically be the same for the native and the lower frequency half of the EDI peak– and thus could work for drifts of all time scales. This is because the nonfringing (ordinary) spectrum, and fringing complex spectrum are both recorded simultaneously in the same fringing spectrum data, and separated during data analysis. (For the former one sums over phase steps to cancel fringing component, for the latter one subtracts phase steps to cancel the ordinary spectrum.)

7.3 Artificially Applied Insults for the Demo

The reason we artificially apply the insult to all channels of the data in the demo in this report is that we lack an experimental multiple-delay data set where we can be sure the same drift was present for all delays. At the time of the last multiple-delay data taking of the T-EDI project, in 2011, we had not yet conceived of the crossfading technique, and thus were unaware of the need to take data in pairs of delay in rapid succession. Instead we took many exposures sitting on a single delay, and then moved to the next delay, and so on. There was significant drift between delays of order 0.4 cm^{-1} per hour (see Fig. 36 of Ref. 3). This drift was removed during analysis by conventional means, by comparing measured to theoretical ThAr lamp spectra.

Then after crossfading was developed, for the demonstrations of this report we used that already aligned data set as a starting point, and manually applied a drift Δx to all delay channels of the data. Then we used our working-code to Fourier process the moiré data, which reverses the heterodyning and sums the wavelets to form an output spectrum. It was our usual working software but with added code to apply a frequency dependent weight prior to the summation.

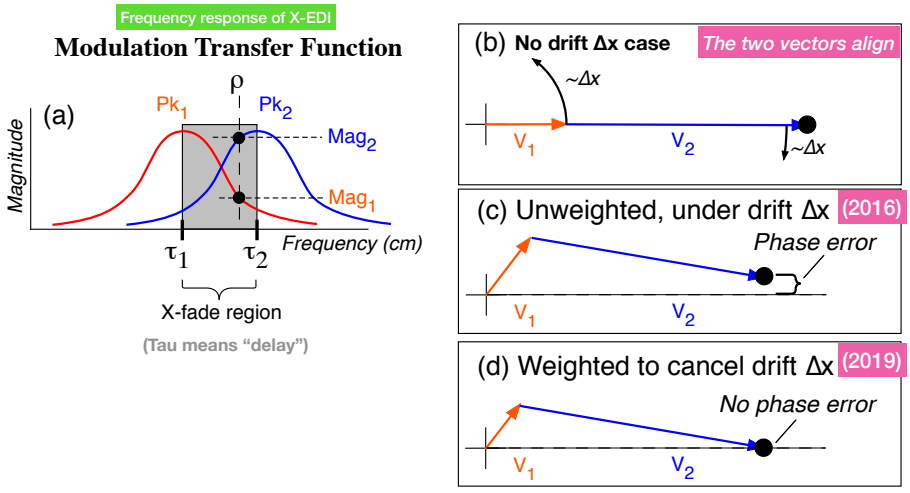

Figure 18. (a) Two overlapping sensitivity peaks in the Modulation Transfer Function of the EDI, one for each delay at τ_1 and τ_2. These twist in opposite directions in response to a drift Δx, and can be made to cancel if weights are chosen appropriately. (b) Virgin position for $\Delta x = 0$, depicted as zero for clarity but in reality can have a small angle which is removed during equalization. (c,d) The vector sum of V_1 and V_2 have lengths Mag_1 and Mag_2 set by the peak height at ρ, and angles by Δx proportional to $(\rho - \tau_n)$. (c) The unweighted sum (as in the 2016 result Fig. 13) shows a reduction, but not perfect cancellation. (d) After weighting by w_1 and w_2, the sum vector is zero (as in the 2019 result Fig. 14). This only works when the two components rotate in opposite directions to Δx, which only occurs when ρ is between τ_1 and τ_2. (In the Figures, delay and frequency have the same units of cm and the horizontal axis is interchangeably labeled.)

7.4 Iteration

We envision that iterating one or two times would benefit crossfading when the insult is large. After the first pass a large insult would be significantly reduced so that on a subsequent pass it would produce smaller phase angle shifts, which more accurately follow a linear behavior to the sine function (the imaginary part of $e^{i2\pi(\Delta x)(\rho-\tau)}$). This produces the best stability gain, working well over a range of Δx.

8. CONCLUSIONS

All spectrographs suffer drift insults of various kinds, and the crossfading-EDI technique reduces the *reaction* to insults in the output spectrum dramatically by moving the duty of fine wavelength determination from the dispersive spectrograph to the interferometer. An interferometer can be added in series with most dispersive spectrographs to form an EDI. We recommend having at least two delays to perform crossfading during analysis. These improvements can boost the performance of the system dramatically over the spectrograph used alone. The stability is boosted from one to three orders of magnitude, and this boost multiplies stability gain G_{conv} from conventional mitigations (which reduces Δx), as $\delta\nu_{out} = \Delta x(1/G_{conv})(1/G_{edi})$. The spectral resolution can be boosted by a factor 2 to 20x, and the robustness to fixed pattern noise dramatically increased. The cross-fading EDI technique allows dramatically smaller, lighter spectrographs to achieve the same stability and resolution tolerances. This can benefit ultra-stable spectrographs for Doppler exoplanet characterization, long term cosmic redshift measurements, improved stability for compact spectrographs used for Raman spectroscopy and biomedical analysis, and for remote sensing spectrographs on air- and space-borne platforms where weight & volume are critically limited.

The downsides are increased number of exposures (more readout noise), increased parasitic reflections from more optics (which diminishes flux and increases photon noise), and more complicated data analysis. However, in many conventional spectrographs the precision is not limited by photon noise but dominated by PSF drift Δx. In this case the small sacrifice in flux in using EDI reduces the net noise by removing a dominating drift noise component.

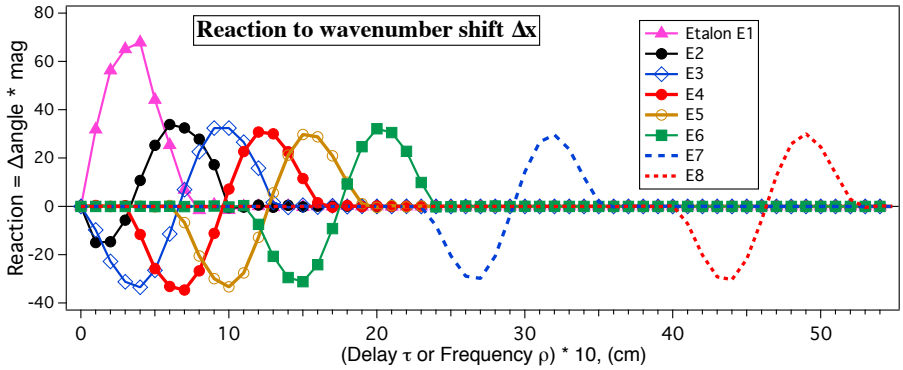

Figure 19. Calculated reaction of the ersatz calibration line (4764 cm^{-1}) to a test wavenumber insult of 0.5 cm^{-1}, for all the etalons of the set. This is a computational intermediate step in computing the optimal weights, which are then applied to the subject line (4849 cm^{-1}). We used our working-code to produce the reconstructed output spectrum, but isolated each etalon's contribution, and then computed the change in Fourier transform for a given Δx. Note the "S" like response versus ρ that crosses zero at the delay (except for the lowest delays where negative frequency energy reflects into positive branch). Etalons E1 - E8 have delays of 0.083, 0.34, 0.66, 0.96, 1.27, 1.75, 2.92, 4.63 cm. Horizontal scale in 0.1 cm units, i.e. the 4.63 cm E8 curve crosses zero at position 46. The vertical axis is reaction, defined as magnitude times angular change in complex plane. The highest two delays E7 and E8 are not currently used for crossfading, since they do not overlap other delays due to gaps in coverage (these were used for highest sensitivity Doppler measurements on M-stars during the T-EDI project[1]). Usage of more delays would in principle allow their inclusion and more than double the available resolution. We include E7 and E8 in the wavelet graphics as an aid to the eyes.

Results of this technique will greatly improve spectral precision and stability for at least two important, and complementary, methods of habitable exoplanet search currently limited by instrument stability or spectral resolution: (1) Doppler radial velocimetry using high resolution spectrographs, by removing instrument noise so that the net precision is limited only by photon noise, and (2) direct planet imaging using adaptive optics (such as the Gemini Planet Imager[5]) that could analyze exoplanet atmospheres with a low resolution integral field multi-object spectrograph, boosted in both resolution and stability by a crossfading-EDI.

ACKNOWLEDGMENTS

This work performed under the auspices of the U.S. Department of Energy by Lawrence Livermore National Laboratory under Contract DE-AC52-07NA27344.

REFERENCES

[1] Muirhead, P. S., Edelstein, J., Erskine, D. J., Wright, J. T., Muterspaugh, M. W., Covey, K. R., Wishnow, E. H., Hamren, K., Andelson, P., Kimber, D., Mercer, T., Halverson, S. P., Vanderburg, A., Mondo, D., Czeszumska, A., and Lloyd, J. P., "Precise Stellar Radial Velocities of an M Dwarf with a Michelson Interferometer and a Medium-Resolution Near-Infrared Spectrograph," *PASP* **123**, 709 (June 2011).

[2] Erskine, D. J., Edelstein, J., Muirhead, P., Muterspaugh, M., Covey, K., Mondo, D., Vanderburg, A., Andelson, P., Kimber, D., Sirk, M., and Lloyd, J., "Ten-fold spectral resolution boosting using TEDI at the Mt. Palomar NIR Triplespec spectrograph," in [*UV/Optical/IR Space Telescopes and Instruments: Innovative Technologies and Concepts V*], Tsakalakos, L., ed., *Proc. SPIE* **8146** (2011).

[3] Erskine, D. J., Edelstein, J., Wishnow, E. H., Sirk, M., Muirhead, P. S., Muterspaugh, M. W., Lloyd, J. P., Ishikawa, Y., McDonald, E. A., Shourt, W. V., and Vanderburg, A. M., "High-resolution broadband spectroscopy using externally dispersed interferometry at the Hale telescope: part 1, data analysis and results," *Journal of Astronomical Telescopes, Instruments, and Systems* **2**, 025004 (Apr. 2016).

[4] Erskine, D. J., Edelstein, J., Wishnow, E., Sirk, M., Muirhead, P. S., Muterspaugh, M. W., and Lloyd, J. P., "High-resolution broadband spectroscopy using externally dispersed interferometry at the Hale telescope: part 2, photon noise theory," *Journal of Astronomical Telescopes, Instruments, and Systems* **2**, 045001 (Oct. 2016).

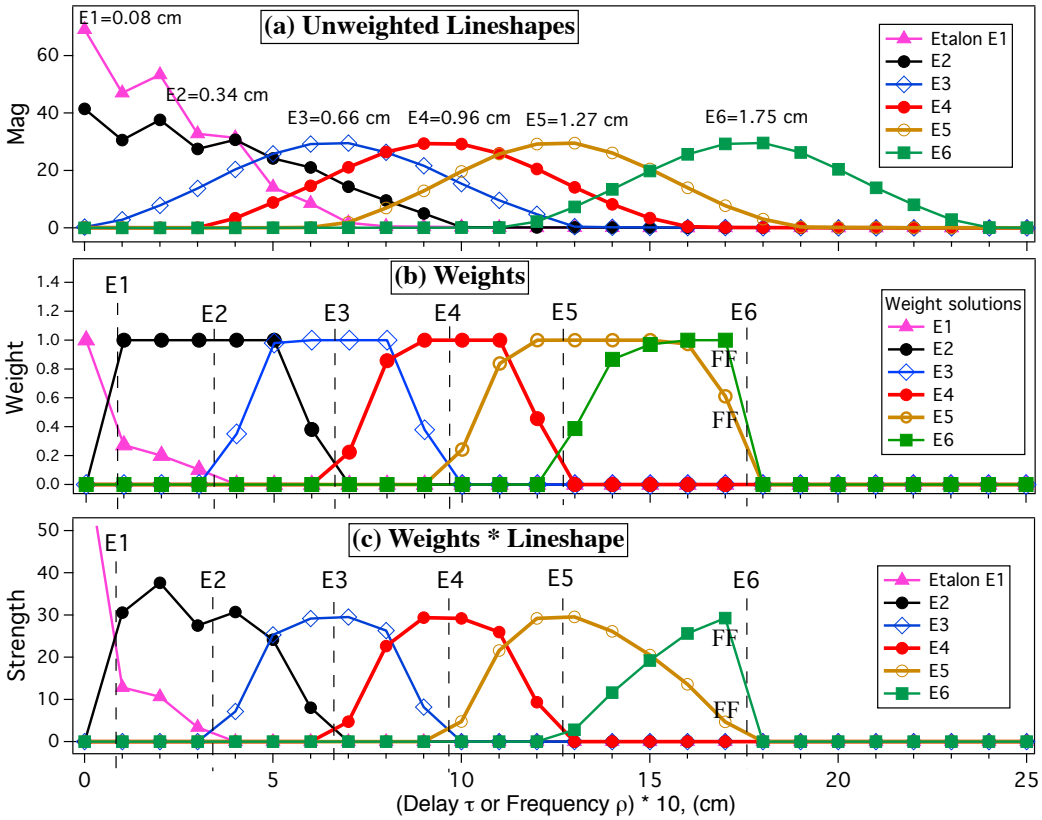

Figure 20. (a) Unweighted lineshapes. (b) Weight solutions (for the -0.5 to 0.5 cm^{-1} case of Δx) that produced phase shift cancellation. The sum vector of each pair of overlapping reaction peaks (of a set E1 - E6) evaluated at each ρ, maintains its original phase. (The contribution of any third overlapping peak was ignored for algorithmic simplicity.) (c) Modified lineshapes after multiplication by weights. E6 does not have an overlapping delay neighbor to its high side, and thus its weight must cut off abruptly at its center 1.8 cm to avoid a Δx dependence.

[5] Macintosh, B. A., Graham, J. R., Palmer, D. W., Doyon, R., Dunn, J., Gavel, D. T., Larkin, J., Oppenheimer, B., Saddlemyer, L., Sivaramakrishnan, A., Wallace, J. K., Bauman, B., Erickson, D. A., Marois, C., Poyneer, L. A., and Soummer, R., "The Gemini Planet Imager: from science to design to construction," in [*Adaptive Optics Systems*], *Proc. SPIE* **7015**, 701518 (July 2008).

[6] Wolff, S. G., Ward-Duong, K., Zalesky, J., Greenbaum, A. Z., Perrin, M. D., and Graham, J., "Gemini planet imager observational calibration XIII: wavelength calibration improvements, stability, and nonlinearity," in [*Ground-based and Airborne Instrumentation for Astronomy VI*], *Proc. SPIE* **9908**, 990838 (Aug. 2016).

[7] Erskine, D. J., Muirhead, P., Vanderburg, A., and Szentgyorgyi, A., "Enhanced exoplanet biosignature detection from an interferometer addition to low resolution spectrographs," in [*Ground-based and Airborne Instrumentation for Astronomy VII*], Evans, C. J., Simard, L., and Takami, H., eds., *Proc. SPIE* **10702**, 1348 – 1354 (Aug. 2018).

[8] Fischer, D. A., Anglada-Escude, G., Arriagada, P., et al., "State of the Field: Extreme Precision Radial Velocities," *Proc. Astr. Soc. Pacific* **128**, 066001 (June 2016).

[9] Erskine, D. J., "Combined dispersive/interference spectroscopy for producing a vector spectrum," *US Patent* **6,351,307** (Issued Feb. 26, 2002).

[10] Erskine, D. J. and Ge, J., "Novel Interferometer Spectrometer for Sensitive Stellar Radial Velocimetry," in [*Imaging the Universe in Three Dimensions: Astrphys. Advncd. Multi-Wavel. Imaging Devices*], van Breugel, W. and Bland-Hawthorn, J., eds., *ASP Conf. Series* **195**, 501–507 (2000).

[11] Erskine, D. J., "An Externally Dispersed Interferometer Prototype for Sensitive Radial Velocimetry: Theory and Demonstration on Sunlight," *PASP* **115**, 255–269 (Feb. 2003).
[12] Erskine, D. J., Edelstein, J., Feuerstein, W. M., and Welsh, B., "High-Resolution Broadband Spectroscopy Using an Externally Dispersed Interferometer," *ApJ* **592**, L103–L106 (Aug. 2003).
[13] Erskine, D. J. and Edelstein, J., "Interferometric resolution boosting for spectrographs," in [*Ground-based Instrumentation for Astronomy*], Moorwood, A. and Iye, M., eds., *Proc. SPIE* **5492**, 190–199 (2004).
[14] Edelstein, J. and Erskine, D. J., "High resolution absorption spectroscopy using externally dispersed interferometry," in [*UV, X-Ray, and Gamma-Ray Space Instrumentation for Astronomy XIV*], Siegmund, O. H. W., ed., *Proc. SPIE* **5898**, 297–307 (Aug. 2005).
[15] Edelstein, J., Muterspaugh, M. W., Erskine, D. J., Marckwordt, M., Feuerstein, W. M., Mercer, T., Czeszumska, A., Schwer, J., Halverson, S., Lloyd, J. P., Muirhead, P. S., Wright, J. T., and Herter, T., "Dispersed interferometry for infrared exoplanet velocimetry," in [*Ground-based and Airborne Instrumentation for Astronomy*], McLean, I. and Casali, M., eds., *Proc. SPIE* **7014** (2008).
[16] Erskine, D. J., "Dispersed interferometers," in [*The WSPC Handbook of Astronomical Instrumentation*], Burrows, D. N. and Moore, A. M., eds., **Vol. 3**, World Scientific Publishing Company, Singapore, https://doi.org/10.1142/9446, ISBN = 978-981-4644-31-0 (February 2021).
[17] Ge, J., van Eyken, J., Mahadevan, S., DeWitt, C., Kane, S. R., Cohen, R., Vanden Heuvel, A., Fleming, S. W., Guo, P., Henry, G. W., Schneider, D. P., Ramsey, L. W., Wittenmyer, R. A., Endl, M., Cochran, W. D., Ford, E. B., Martín, E. L., Israelian, G., Valenti, J., and Montes, D., "The first extrasolar planet discovered with a new-generation high-throughput Doppler instrument," *ApJ* **648**, 683–695 (2006).
[18] Ma, B., Ge, J., Wolszczan, A., Muterspaugh, M. W., Lee, B., Henry, G. W., Schneider, D. P., Martín, E. L., Niedzielski, A., Xie, J., Fleming, S. W., Thomas, N., Williamson, M., Zhu, Z., Agol, E., Bizyaev, D., da Costa, L. N., Jiang, P., Fiorenzano, A. F. M., Hernández, J. I. G., Guo, P., Grieves, N., Li, R., Liu, J., Mahadevan, S., Mazeh, T., Nguyen, D. C., Paegert, M., Sithajan, S., Stassun, K., Thirupathi, S., van Eyken, J. C., Wan, X., Wang, J., Wisniewski, J. P., Zhao, B., and Zucker, S., "Very low-mass stellar and substellar companions to solar-like stars from MARVELS. VI. a giant planet and a brown dwarf candidate in a close binary system HD 87646," *Astronomical Journal* **152**, 112 (Oct. 2016). 10.3847/0004-6256/152/5/112.
[19] van Eyken, J. C., Ge, J., and Mahadevan, S., "Theory of Dispersed Fixed-delay Interferometry for Radial Velocity Exoplanet Searches," *ApJS* **189**, 156–180 (2010).
[20] Ge, J., Erskine, D. J., and Rushford, M., "An Externally Dispersed Interferometer for Sensitive Doppler Extrasolar Planet Searches," *PASP* **114**, 1016–1028 (Sept. 2002).
[21] Kim, A. G., Linder, E. V., Edelstein, J., and Erskine, D., "Giving cosmic redshift drift a whirl," *Astroparticle Physics* **62**, 195–205 (Mar. 2015).
[22] Erskine, D., Buschmann, M., Easther, R., Ferraro, S., Kim, A., Linder, E., Muirhead, P., Phillips, D., Ravi, A., Safdi, B., Schaan, E., Silverwood, H., and Walsworth, R., "Direct Acceleration: Cosmic and Exoplanet Synergies," *Bulletin of the American Astronomical Society* **51**, 53 (May 2019).
[23] Behr, B. B., Cenko, A. T., Hajian, A. R., McMillan, R. S., Murison, M., Meade, J., and Hindsley, R., "Stellar Astrophysics with a Dispersed Fourier Transform Spectrograph. II. Orbits of Double-lined Spectroscopic Binaries," *AJ* **142**, 6 (July 2011).
[24] Harlander, J., Reynolds, R., and Roesler, F., "Spatial Heterodyne Spectroscopy for the Exploration of Diffuse Interstellar Emission Lines at Far-ultraviolet Wavelengths," *ApJ* **396**, 730 (1992).
[25] Erskine, D. J. and Linder, E. V., "A 1000x stabler spectrograph using an interferometer with crossfaded delays," in [*OSA Optical Sensors, Fourier Transform Spectroscopy Topical Mtg.*], *OSA Optical Sensors, Fourier Transform Spectroscopy Topical Mtg.* , FW5B.3, Optical Society of America (June 2019).
[26] Wilson, J. C., Henderson, C. P., Herter, T. L., Matthews, K., Skrutskie, M. F., Adams, J. D., Moon, D.-S., Smith, R., Gautier, N., Ressler, M., Soifer, B. T., Lin, S., Howard, J., LaMarr, J., Stolberg, T. M., and Zink, J., "Mass producing an efficient NIR spectrograph," in [*Ground-based Instrumentation for Astronomy*], Moorwood, A. and Iye, M., eds., *Proc. SPIE* **5492**, 1295–1305 (2004).
[27] Kerber, F., Nave, G., and Sansonetti, C. J., "The Spectrum of Th-Ar Hollow Cathode Lamps in the 691-5804 nm region: Establishing Wavelength Standards for the Calibration of Infrared Spectrographs," *ApJS* **178**, 374–381 (2008).